A Coupled Numerical Investigation of the Cape Fear River Basin during Hurricane Florence (2018)

Dongxiao Yin,[1] Z. George Xue,[1,2,3*] Daoyang Bao,[1] Arezoo RafieeiNasab,[4] Yongjie Huang,[5] Mirce Morales[6]

1 Department of Oceanography and Coastal Sciences, Louisiana State University, Baton Rouge, LA 70803, USA

2 Center for Computation and Technology, Louisiana State University, Baton Rouge, LA 70803, USA

3 Coastal Studies Institute, Louisiana State University, Baton Rouge, LA 70803, USA

4 National Center for Atmospheric Research, Research Applications Laboratory, Boulder, CO 80305, USA

5 School of Meteorology, University of Oklahoma, Norman, OK 73072, USA

6 School of Engineering, National Autonomous University of Mexico, Mexico City, CP 04510, Mexico

Corresponding Author: Department of Oceanography and Coastal Sciences, Louisiana State University, Baton Rouge, LA 70803, USA; zxue@lsu.edu

Abstract

In this study we adapted WRF-Hydro to the Cape Fear River basin (CFRB) to assess its performance during Hurricane Florence (2018). The model was first calibrated with a strategy of mixture of automatic and manual calibration during Florence and then evaluated with an independent hurricane event. With satisfactory NSE values (>0.4) achieved at all gages for hourly simulation, the model demonstrates its potential in simulating the flood response at both basin and sub-basin scale during hurricane events. The model's capability in reproducing rainfall and properly translating it to hydrological response was further evaluated. The analysis suggests that the calibrated WRF-Hydro in combination with a series of WRF simulation using different microphysics schemes can provide reasonable flood simulations. The model reproduced peak streamflow observed at gage stations with acceptable errors in timing and amplitude. Meanwhile, positive(negative) bias in rainfall input is likely to be amplified (reduced) in streamflow forecast when simulated rainfall volume is larger than the "model true". And the timing bias mostly inherited from rainfall simulation and calibration process.

Keywords: WRF, WRF-Hydro, Hurricane Florence, Cape Fear River, Coupling

Introduction

Flooding is the costliest natural disaster in the United States. Over the past 30 years, the annual average economic loss caused by freshwater flooding amounts $8.2 billon (Wing *et al.*, 2018). For United States east coast, a major cause of floods is the landfalling tropical cyclones(Smith *et al.*, 2010; Villarini and Smith, 2010). During 1963 to 2012, hurricane induced inland floods and mudslides accounts for 27% out of 2325 deaths (Rappaport, 2014). Moreover, climate models project an increase in both the intensities of the strongest storms and accompanying rainfall rates (Knutson *et al.*, 2010; Walsh *et al.*, 2016; Dinan, 2017). In light of this, accurate simulation of hurricane induced floods is of vital importance and in urgent need.

Hydrometeorological modeling system provides one best way for flood forecast by integrating both meteorological and hydrologic models. Weather condition is simulated by the meteorological model and then translated into flood response via the hydrological component. One notable example of such systems is the Weather Research and Forecasting Model Hydrological modeling extension package (WRF-Hydro; (Gochis *et al.*, 2020). WRF-Hydro is a physically based and fully distributed hydrometeorological system developed by National Center for Atmospheric Research (NCAR) in the United States. WRF-Hydro can be driven by independent meteorological data (e.g. Phase 2 of the North American Land Data Assimilation System, [NLDAS2], (Mitchell *et al.*, 2004; Xia *et al.*, 2012) and supports both one-way and two-way coupling with the Weather Research and Forecasting Model (WRF). Researchers have applied WRF-Hydro in offline mode to study hydrologic cycle and water resource management (Somos-Valenzuela and Palmer, 2018), hydroclimatic change (Xue *et al.*, 2018), sediment transport (Yin *et al.*, 2020) and re-infiltration process (Zhang *et al.*, 2020). Driven by meteorological variable simulated by WRF, WRF-Hydro has also been used to conduct water budget analysis (Li *et al.*, 2017; Kerandi *et al.*, 2018), to investigate costal ocean's effect on hydrological simulation (Senatore *et al.*, 2020a, 2020b), and to reconstruct river runoff (Verri *et al.*, 2017). In addition, WRF-Hydro can be fully coupled with WRF, in which the feedback between atmosphere and lateral and vertical redistribution of soil moisture are resolved (Senatore *et al.*, 2015; Kerandi *et al.*, 2018; Rummler *et al.*, 2019; Fersch *et al.*, 2020).

Since its first release in 2015, WRF-Hydro has been used to study flooding events induced by various mechanisms of precipitation (Ryu *et al.*, 2017; Lin *et al.*, 2018b; Papaioannou *et al.*, 2019; Li *et al.*, 2020; Viterbo *et al.*, 2020). WRF-Hydro also serves as the core component of the National Oceanic and Atmospheric Administration National Water Model (NOAA NWM) in the United States, and of the Operational Flood Forecasting system operated by Israeli Hydrological Service in Israel. Nevertheless, few studies investigate the WRF-Hydro's utility of simulating hurricane induced flood so far.

We adapted WRF-Hydro over the Cape Fear River Basin (CFRB) during Hurricane Florence (Florence, 2018) to evaluate its performance in simulating hurricane induced flooding events. For this, the model was firstly calibrated and evaluated driven by existing meteorological dataset. We then coupled (one-way) WRF with WRF-Hydro to assess its skill and investigate the error interaction during the modeling chain process. The rest of the paper is organized as follows. Section 2 describes material and methods, including study area information, model framework as well as calibration and evaluation methodology. Section 3 discusses the performance of WRF-Hydro system in offline mode along with the calibration results. Section 4 presents the coupling between WRF and WRF-Hydro system. In Section 5, we close the paper with summary and conclusions.

2. Material and methods

2.1 Cape Fear River Basin

The Cape Fear River is a blackwater river with a length of 320km in the east central of North Carolina. Formed from the confluence of the Haw River and Deep River, it is joined by the Little River and Black River, as well as the Northeast Cape Fear River (NE CFR hereafter) as it flows southeastward towards the Atlantic Ocean (Figure 1b). In total, the Cape Fear River drains an area of 23,889 km^2, forming the CFRB as the largest river basin entirely contained in North Carolina's borders.

The climate over the basin is subtropical with long, hot, humid summers and short, cold to mild winters. During 2002 to 2012, the average precipitation is estimated to be around 1200 mm (Hamel and Guswa, 2015). July and August are the months of maximum rainfall owing to the isolated, convective-type storms. Minimum monthly rainfall comes in April over the upstream area, and October to November for downstream area.

Based on physiographic characteristics, the CFRB can be divided into upper, middle and lower part. The upper CFRB contains 2 USGS HUC 8 watersheds-HUC 03030002 and HUC 03030003 (Figure 1c)- and features rolling and hilly landscape. The middle CFRB includes only HUC 03030004 and is characterized by rolling terrain with little relief. Composed of HUC 03030005, HUC 03030006 and HUC 03030007 (Figure 1c), the lower CFRB flattens out to be nearly level (Alford *et al.*, 2016).

According to the 21 Category Modified International Geosphere Biosphere Programme (IGBP) Moderate Resolution Imaging Spectrometer (MODIS) land cover product, there are 16 types of land cover over the CFRB. The dominating land use types are cropland/natural vegetation mosaic (32%), mixed forests (20%), deciduous broadleaf forest (18%). Besides that, Croplands and Urban and Built-up accounts for 6.8% and 3.5% over the whole basin. The soil types are mainly sandy loam (33.6%), loamy sand (24.2%), sand (22.1%), silt loam (11.9%) and loam (7.1%) according to the State Soil Geographic Database (Miller and White, 1998).

Human management also plays a key role in modifying streamflow response in the CFRB. There are around 1,100 impoundments with dams over the basin, the majority of which are in the upper part (Curtis Weaver *et al.*, 2001). Among them, the largest surface area impoundment is the B. Everett Jordan Lake (Jordan Lake hereafter, Figure 1b). Located at 7km upstream of the mouth of the Haw River, it covers an area of 56.4 km^2. The major purpose served by Jordan Lake is to provide flood damage reduction. Along the Deep River and mainstream of Cape Fear River, there are a series of small dams (Figure 1b). Those dams are typically operated on the basis of "run-of-river" mode in which outflows from them are almost equal to inflows to them (Weaver and Carolina, 1997).

2.2 Hurricane Florence

Florence originated from a tropical wave over Western Africa and intensified to a tropical depression around 1800 UTC 31, August 2018. It strengthened into a tropical storm 12 hours later and became a Category 1 hurricane at 0000 UTC 04, September 2018. And 42 hours later, Florence intensified into a category 4 hurricane before weakening into a tropical storm at 0000 UTC 7 September. By 1200 UTC 09 September, it restrengthened into the hurricane category and began moving in the west-northwest direction. Florence made landfall as a category 1 hurricane near Wrightsville Beach, North Carolina around 1115 UTC 14 September. After that, it degraded into a tropical storm by 0000 UTC 15 and a tropical depression at 1800 UTC 16 September. The hurricane finally dissipated by 1800 UTC 18, September 2018.

Florence brought historic amounts of rainfall across the CFRB with a new record rainfall total of 912 mm (Figure 1d) from a tropical system. Severe flooding happened following the rainfall. Ten USGS Gages observed new records of peak streamflow, at three of which the estimated Annual Exceedance Probability was equal or less than 0.2%, which corresponds to a 500-year or greater flood event (Feaster *et al.*, 2018).

2.3 WRF-Hydro System

The *WRF-Hydro system* contains two main components: the atmospheric model WRF and the hydrological model WRF-Hydro. We here present the setup and configurations of the WRF-Hydro system and numerical experiments in this study.

2.3.1 WRF

In this study, the Advanced Research Version of WRF Version 4.0.1 (UCAR, 2019) developed by NCAR was applied to simulate the weather condition and to provide forcing for the hydrological model. WRF is a non-hydrostatic, meso-scale model and has been a flagship weather forecast model in meteorology.

As shown in Figure 2, a one-way nested domain was built for WRF with a grid space ratio of 3. The outer domain (WRF D01) covers the eastern, middle and southern United States as well as the Gulf of Mexico with a grid spacing of 9 km. The inner domain (WRF D02) includes North and South Carolina with a 3 km grid resolution. The vertical levels were 40 for both domains. The Yonsei State University scheme (YSU, Hong *et al.*, 2006), the RRTM Model for GCMs (RRTMG, Iacono *et al.*, 2008), the revised MM5 Monin-Obukhov surface layer scheme and the unified Noah-MP land-surface model (Niu *et al.*, 2011a) were selected for both domains. In addition, Tiedtke scheme was only applied for the outer domain (WRF D01).

Initial and boundary conditions for the simulation were taken from the fifth generation European Centre for Medium-Range Weather Forecasts (ECMWF) atmospheric reanalysis of the global climate (ERA5) with hourly interval. Its horizontal resolution is 0.25°. WRF simulation was initiated at 0018 UTC 13 September 2020, which is about 24 hours before Florence made landfall and ended at 0600 UTC 18 September 2018.

Table 1 details the setup of the numerical experiments conducted in this study. Experiments OFF1, OFF2 and OFF3 were designed for the one-way coupled evaluation. In these three experiments, WRF was applied with Single-Moment 6-class (WSM6, Hong *et al.*, 2005), Thompson graupel (Thompson, Thompson *et al.*, 2008) and Morrison (Morrison, Morrison *et al.*, 2009) microphysics schemes, respectively, as an ensemble.

Hourly output from the inner domain (WRF D02) was then regridded to 1 km over the WRF-Hydro domain (WH D01) to provide forcing for the following hydrologic simulation.

2.3.2 WRF-Hydro

As the hydrological component, WRF-Hydro V5.1.1 (Gochis *et al.*, 2020) was used in this study to investigate the flood response during Florence. Built upon the Noah land surface model with multi-parameterization options (Noah-MP, Niu *et al.*, 2011a), WRF-Hydro enhances the physical realism of water cycle by integrating subsurface and overland flow routing, base flow and channel routing via corresponding modules. In our study, subsurface routing, one-way overland routing, the bucket base flow model as well as diffusive wave routing are all applied. The computational domain of WRF-Hydro (WHD01) has a dimension of 2490 (west to east) × 3490 (north to south) with a 100 m horizontal resolution (Figure 1b, Figure 2), which is 10 times finer than that of Noah-MP. The timestep of Noah-MP is set to one hour while that of overland and channel routing is 10 seconds in the hydrological simulation.

2.4 Calibration of WRF-Hydro

To obtain a sound simulation, WRF-Hydro needs to spin up, carefully calibrated and rigorously evaluated in sequence. We followed this procedure to first determine the proper length of needed spin-up time prior to calibration. Following (Cai *et al.*, 2014), the minimum spin-up time required is defined at the N months when

$$|Var^{N+1} - Var^{N}| < 0.001 * |Var^{N}| \quad (1)$$

where Var stands for the variable used to estimate the spin-up time needed, in our study the column averaged soil moisture is selected according to previous study (Li *et al.*, 2020). The result is presented in Section 3.1.

Table 2 details the methodology applied for calibration. To the end of a satisfactory model performance over the entire basin, calibration was conducted on all the major tributaries and the mainstem of the Cape Fear River in a cascade way. For the tributaries, the USGS gages that is closest to the mouth of the river basin and out of the influence of oceanic processes are selected for calibration purpose. Here, we choose USGS gage at Bynum (USGS gage 02096960), Moncure (USGS gage 02102000), Manchester (USGS gage 02103000), Tomahawk (USGS gage 02106500) and Chinquapin (USGS gage 02108000) for the Haw River basin, Deep River basin, Little River basin, Black River basin and the NE CPR basin (see Figure 1b for the location), respectively. Once the calibration for the tributaries was finished, we further calibrated the mainstem of Cape Fear River at Kelly (USGS gage 02105769) (see Figure 1b for the location).

A strategy of a mixture of automatic and manual calibration was chosen. The NE CFR basin, Black River basin and Little River basin were calibrated manually through a stepwise way, while The NCAR's WRF-Hydro calibration tool was applied on the Haw River basin and Deep River basin. The tool makes use of Dynamically Dimensioned Search (DDS) methodology, which is designed for multiple parameters calibration and is ideally suited for fully distributed model such as WRF-Hydro (Tolson and Shoemaker, 2007). For quantitative evaluation of model performance, Nash-Sutcliffe coefficient (NSE, Eq. (2)) was calculated during the processes.

$$NSE = 1 - \frac{\sum_{t=1}^{T} \left(O_t - P_t\right)^2}{\sum_{t=1}^{T} \left(P_t - \overline{O_t}\right)^2} \quad (2)$$

where O_t is the measured streamflow at time t, P_t is simulated streamflow at time t, $\overline{O_t}$ is the mean of measured streamflow. Following (Lin *et al.*, 2018a), a NSE value of > 0.4 is considered as satisfactory for simulated hourly streamflow under heavy rainfall events. Once calibrated, the parameters are concatenated and distributed spatially over the CFRB. Evaluation is carried out after calibration over independent event to assess the transferability of the calibrated parameters.

During the calibration and evaluation in offline mode, the precipitation forcing is regridded from the Stage IV multi-sensor quantitative precipitation estimation product (Stage IV), which provides hourly rainfall rate at a 4km resolution over the conterminous United States (Lin, 2011). Other forcing variables including air temperature, wind, short and long wave radiation, humidity and pressure are from NLDAS2. The results of model calibration and evaluation in offline mode are presented in Section 3.2~3.3.

3. Spin-up, calibration and evaluation of WRF-Hydro system in offline mode

3.1 Spin-up

Prior to calibration, we performed 17 experiments with spin-up windows varying from 1 to 17 months to determine the sufficient length of spin-up time needed for model to reach the equilibrium. We calculated the basin and column averaged soil moisture over CFRB and the relative difference ($\left|Var^{N+1} - Var^{N}\right|$) between each experiment using Eq. (1). As is shown in Figure 3, significant difference exists among neighboring experiments when spin-up time is less than 3 months. Such variation gets smaller as the spin-up time increases. Once spin-up for 8 months and longer, the model reaches the equilibrium condition where the difference between neighboring experiments is less than 0.001. Thus, we confirm that 8-month is sufficient for spin-up purpose.

3.2 Calibration

3.2.1 The Black River

A stepwise approach was applied for calibration over the Black River at Tomahawk (USGS gage 02106500, see Figure 1b for location) following (Yucel *et al.*, 2015). The infiltration scaling parameter (*refkdt*) which highly influences the partition between infiltration and surface runoff was calibrated first. Nine numerical experiments were carried out with *refkdt* of 0.1, 0.2, 0.4, 0.8, 1.0, 1.5, 2.0, 2.5, 3.0, respectively. The simulation results are shown in Figure 4a~b. Model performance improves as the *refkdt* increases and the best skill is achieved at a value of 3.0.

Considering the difference between observed and simulated peaking time, we further calibrated the speed of overland flow by adjusting the overland roughness parameter (*OVROUGHRTFAC*). In WRF-Hydro, an increase (decrease) of *OVROUGHRTFAC* will lead to decrease (increase) of the velocity of overland flow, resulting in the delay (advancing) of peak flow. Meanwhile, an increase (decrease) in the speed of overland flow may decrease (increase) the volume of streamflow by decreasing (increasing) the re-infiltration during lateral movement of surface runoff.

We conducted five numerical experiments with the *OVROUGHRTFAC* values of 0.01, 0.1, 1, 10 and 100, respectively. Figure 4c compares the simulated hydrographs against the observed ones. Model performance in both timing and amplitude improves as *OVROUGHRTFAC* increases (Figure 4d). With the maximum value of *OVROUGHRTFAC* at 100, model reaches optimal skill with residual timing bias. Additional experiments indicate that larger values of OVROUGHRTFAC (10000 and 100000, not shown), which are out of the normal range, cannot further alleviate the timing difference. This suggests that this residual timing error might be attributed to the model's inaccurate representation of channel flow. Thus, we further calibrated the manning coefficient of channel (*MannN*).

We designed five experiments in which the manning coefficient of the channels is set to be 1, 2, 3, 4, 5 times of the default value, respectively, with a *refkdt* of 3.0 and the *OVROUGHRTFAC* of 100. Figure 4e~f shows the simulated hydrographs and the NSE-*MannN* relationship. Timing of the simulated hydrograph is sensitive to the manning coefficient. Increasing *MannN* will decrease the flow velocity thus delaying the peaking time. The best model performance (NSE=0.98) is achieved with the value of manning coefficient three times of the default, i.e., *MannN equals three*.

3.2.2 The Northeast Cape Fear River and Little River

Following the calibration over Black River basin, the model was further calibrated over the NE CFR Basin and Little River Basin at Chinquapin (USGS gage 02108000) and Manchester (USGS gage 02103000), respectively. For the sake of computational efficiency, we applied the calibrated parameters for the Black River basin to these two basins prior to the calibration. Figure 5 compares the simulated hydrographs against observed ones at the two gages. An NSE value of 0.79 at Chinquapin (USGS gage 02108000) (Figure 5a) indicates the transferability of the calibrated parameters to the NE CFR basin. This, however, is reasonable considering the hydrologic similarity between NE CFR and Black River basin. Additional calibration was thus not carried out for the NE CFR basin.

On the other hand, for Little River at Manchester (USGS gage 02103000) (Figure 5b), the amplitude and overall shape of the modeled hydrograph matches well with the observed one. An NSE value of 0.48 is also regarded as a satisfactory performance while timing difference exists. To alleviate this, the manning coefficient of channel roughness needs to be readjusted for Little River basin. However, in the original WRF-Hydro, Strahler stream order is used to organize the channel element. Channel grids with the same stream order are assigned with uniform values of channel parameters. This design is in essence not compatible with the grid-based signature of the model. Such channel algorithm only allows for the calibration of the channel parameters within a drainage basin as a whole, while may fail to account for the spatial heterogeneity of channel characteristics over large costal watersheds like CFRB. In this case, we would suggest future improvement of WRF-Hydro to support grid-based or sub-basin wise channel parameters to better consider the spatial variation of flood response. To prove the potential benefit of such modification, we here changed the *manning roughness parameter* from being stream-order uniform to be sub-basin wise distributed. Based on this change, we readjusted the channel parameters over the Little River basin while keeping those over the other part of the basin unchanged. Shown in Figure 5c, a much better model performance is achieved with an NSE value of 0.80 when *MannN* equals 1.

3.2.3 The Haw River

Calibration for the Haw River basin is conducted on the USGS Gage at Bynum (02096960, Figure 1b). We first used the calibrated parameters for the Black River and Little

River basin to check if they can be transferred to the Haw River basin. Figure 6a compares the simulated and observed hydrographs. Regardless of the parameters used, simulated hydrographs exhibit great discrepancy with observed one. This indicates the significant difference of hydrologic controls on the flood response between those three sub-basins. Thus, we conducted an independent calibration over the Haw River basin.

Prior to calibration, the most sensitive parameters were determined via numerical experiments. As a result, the *LKSATFAC, OVROUGHRTFAC, refkdt* and *slope* are the parameters model performance are most sensitive to and were selected for further calibration (Table 3). With 150 iterations, an optimal NSE value of 0.91 was derived (Figure 6b).

3.2.4 The Deep River

The calibration of the Deep River basin was conducted after that of the Haw River. In view of the hydrological similarity between the two basins, calibrated parameters from the Haw River basin were applied on the Deep River basin prior to calibration. As is shown in Figure 7, the model exhibits satisfactory performance over the two branches of the Deep River at Siler City (USGS gage 02101726) and Ramseur (USGS gage 02100500) (Figure 7a~b, see Figure 1b for gage locations) with NSE of 0.85 and 0.92, respectively. While at the mouth of the basin at Moncure (USGS gage 02102000), simulated hydrograph fails to fit with the shape and timing of the observed (Figure 7c) although the modeled runoff volume is within 10% difference. The observed hydrograph is characterized by two peaks while the simulated only has one. The two-peak shape is caused by the difference in the speed of flood wave advection between areas upstream of Siler City (USGS gage 02101726) and Ramseur (USGS gage 02100500) and that downstream of them. Due to the attenuation effect of flood plain and forest cover, speed of flood wave over the intervening area between the Siler City (USGS gage 02101726) and the mouth of the Deep River basin is much lower than that in the upstream part. As they both propagate downstream to the mouth, the velocity difference led to the occurrence of two peaks and timing difference between them. However, current algorithm of WRF-Hydro cannot simulate either the overbank flow effect or the attenuation effect of floodplain to flood wave transmission. This might result in much higher peak discharge and shorter flood duration forecast than it should be in actual, as the case shown in Figure 7c. And a second significant pulse of flood associated with the second peak could then be missed by the WRF-Hydro system. Advancement of model algorithm to consider the overbank flow and the spatial heterogeneity of channel roughness as mentioned above should be able to enhance model performance in predicting such catastrophic flood response. In this study, to compensate for this, we manually increased the manning coefficient of the channel network over this area based on our change to the code mentioned above. Optimal model result was achieved with a NSE of 0.84 (Figure 7d).

3.2.5 The Cape Fear River

For a grid-based modeling system, satisfactory simulation of flood response can be more challenging at the mainstem than that over the tributaries due to the accumulation of error and uncertainty. For instance, the model performance shown in Figure 8a was not satisfactory with large amplitude and timing error. This is partly due to the lack of consideration of spatial heterogeneity of flood wave transmission as mentioned above. Also, it is attributable to the absence of representation of the flood control effect of the Jordan Lake Dam. Shown in Figure 8b, substantial discrepancy exists between the model simulated hydrograph at the outlet of the Jordan Lake Dam and the human controlled one. This human altered flow, if not considered in the model, would result in overestimation of flood flow downstream of it. Thus, another potential improvement of the WRF-Hydro system would be the consideration of water management, which is a problem frequently encountered over coastal watersheds. In this study, we proposed a simple method by assimilating the human altered flow from Jordan Lake Dam at USGS Gage 02098206 into model simulation. Based on this assimilation, we calibrated the model over the mainstem of the Cape Fear River at Kelly (USGS gage 02105769). The optimal result is shown in Figure 8c with a NSE value of 0.42.

3.3 Model evaluation

3.3.1 Evaluation of Evapotranspiration

To build confidence of WRF-Hydro's performance in water partitioning between different compartments, we evaluated the simulated evapotranspiration (ET hereafter) during Florence. Due to the absence of ground observations, the remotely sensed 8-day ET from the MOD16 A2 Version 6 Evapotranspiration/Laten Flux product at 500m resolution (MODIS ET hereafter , Running *et al.*; Mu *et al.*, 2011) were utilized as reference to validate model's performance following previous studies (e.g., Lin *et al.*, 2018c; Parajuli *et al.*, 2018; Xue *et al.*, 2018).

Table 4 compares the basin average ET during 14 to 30 September 2018 from MODIS and model simulation. The correlation coefficient between modeled and MODIS ET is 0.59, which is in line with previous works (Bowman *et al.*, 2015; Parajuli *et al.*, 2018), implying a reasonable model performance. Meanwhile, it should be noted that model generally overestimated the ET compared to MODIS, which is also reported by Long *et al.*, (2014). However, the overestimation is negligible, which is less than 0.3 mm/d on average over the whole basin.

3.3.2 Evaluation with independent event

To validate the transferability of the calibrated parameters, we further evaluated model's performance during Hurricane Matthew (2016, Matthew hereafter,). As the most powerful hurricane event hitting the CFRB prior to Florence, Matthew formed as a category 5 hurricane at 0000 UTC 1 October 2016. It made land fall around 1500 UTC 8 October along the central coast of South Carolina as a category 1 hurricane (Figure 9a). 3 hours later the center of Matthew moved back to the ocean and kept offshore of costal North Carolina through 9 October. During the two days it passed by the Carolinas, large amount of rainfall was dumped over the CFRB, with the maximum total rainfall of 431mm (Figure 9b). Florence and Matthew are the two major storms dominating the upper tail of the peak flow distribution in CFRB. Before Florence, the record of peak flow over the Cape Fear River at Kelly (USGS gage 02105769) was set by Matthew.

Figure 10 compares the simulated hydrographs against observations over the Cape Fear River and its major tributaries during Matthew. WRF-Hydro in offline mode exhibits satisfactory performance at all the gages. This indicates the ability of the calibrated WRF-Hydro in reproducing flood response over independent hurricane event. Also, it also suggests that a grid-based modeling system like WRF-Hydro is at least able to provide flood forecast with reasonable accuracy at sub-basin scale over a large coastal river basin as long as the forcing input is accurate and the spatial heterogeneity of land surface characters as well as the human effect are approximately considered.

4. Evaluation of WRF- and WRF-Hydro coupling

In this section, the performance of WRF-Hydro system coupled with WRF model in translating the meteorological event to reliable flood forecast is evaluated. In addition, the source and propagation of the model error along the model coupling is also discussed.

4.1 Rainfall simulation

Figure 11 compares the simulated storm total rainfall during 0000 UTC 14 to 0000 UTC 18 September 2018 against the total rainfall of Stage IV. A southwestward displacement of rainband associated with the hurricane is found in all experiments. This is due to the spatial shift of simulated tracks to the oceanside compared to the NOAA best track over the coastal area, where the majority of rainfall was dumped. Similarly, due to the better reproduction of the hurricane track, the rainfall field from the simulation with WSM6 scheme (Figure 11a) exhibits the best agreement with Stage IV among the three experiments (Figure 11b-c).

The areal storm total rainfall for CFRB from the three WRF simulations are 361.6 mm with WSM6 scheme, 253.3 mm with Thompson scheme and 240.1 mm with Morrison scheme, respectively, which are all underestimated compared to that of Stage IV (Figure 1d, 390.6 mm). Figure 12a–c shows the storm total rainfall difference during 0000 UTC 14 to 0000 UTC 18 September 2018 between WRF simulation and Stage IV (simulation subtracted by Stage IV). Overall, all three simulations tend to underestimate the storm total rainfall over the lower part of the CFRB. The maximum underestimate is found over the most downstream part of the basin around the Cape Fear River Estuary. Moreover, the WRF simulation with WSM6 scheme (OFF1) overestimated the precipitation for the middle CFRB while the other two experiments exhibit underestimate. For the upper CFRB, side-by-side couplets of over- and underestimate are found in all simulations, which extend southeastward in Figure 12a from WSM6 scheme whereas are along the northeast direction in Figure 12b–c.

The hourly areal rainfall rates of the simulations and Stage IV at basin and sub-basin scale are shown in Figure 13. The performance statistics are listed in Table 5. Areal rainfall rates exhibit multiple peaks as the result of the storm motion and rainband structure evolution, which can be captured by all WRF simulations. The bias, which ranges from -2.35 to 1.51 mm/h, is relatively small, indicating better skill of the model in reproducing the rainfall amount on average. However, the simulations can hardly capture the hourly variation of the areal rainfall rate. This can be justified by the negative NSE (-0.41 on average), low R^2 (0.17 on average) and large RMSE (4.07 on average) values. In addition, the prediction skill is generally superior in sub-basins upstream over those in the middle and lower CFRB.

4.2 Flood response

In this section we evaluate the performance of WRF-Hydro in reproducing the flood response and discuss the error interaction during the simulation. The flood response is characterized in terms of runoff volume, runoff-to-rainfall ratio, peak discharge as well as the ratio between runoff volume and peak discharge. Figure 14 compares the simulated hydrographs with the observation. Table 6 summarizes the flood response from each simulation and compares them with observations. Here, rainfall volume (mm) was calculated from Stage IV and WRF simulations for the period of 0000 UTC 14 September to 0000 UTC 18 September and divided by drainage areas. Observed runoff volume (mm) was computed by integrating observed discharge over the period of 0000 UTC 14 September to 0000 UTC 24 September 2018 and dividing it by drainage area for the major sub-basins. And is integrated over 0000 UTC 14 September to 0000 UTC 30 September 2018 for the Cape Fear River basin above Kelly (USGS gage 02105769) to make it comparable with the calibration process. The rainfall ratio is the simulated total rainfall divided by the Stage IV counterpart. In the same way, the runoff ratio and peak discharge ratio are calculated for the runoff volume and peak discharge, respectively. Rainfall centroid is used to represent the timing distribution of storm total rainfall, which refers to the time at which 50% of the total rainfall occurs. The timing difference is defined as the mismatch between observation and simulation in time. Negative values indicates that observation is ahead of simulation while positive values implies that the simulation is earlier than actual.

Figure 14 shows the simulated and observed hydrographs over the Cape Fear River and its major tributaries. In general, all simulations can capture the general shape of the observed hydrograph with some timing advance and amplitude errors. A direct WRF-WRF Hydro coupling can effectively translate the meteorological event to the hydrological signal (flood peak). In addition, although the observed peak discharge is over- or under-estimated in any single simulation, it falls within the range of the simulations over all basins except at the Deep River basin (Figure 14d). This implies the necessity and benefit of WRF-simulations with different microphysics schemes. Further, despite the less skillful performance of meteorological inputs from WRF simulation in capturing the temporal variation of rainfall intensity, the NSE values of streamflow simulation (Table 6) is generally better than the corresponding values of hourly rainfall rate (Table 5). This indicates the streamflow response is dominated by the storm total rainfall volume instead of rainfall intensity during Florence over CFRB.

The model's performance in reproducing the flood response also points out the error interaction using a one-way coupled WRF-Hydro. As observed from the modeling results for all the basins except the NE CFR, the rainfall ratio is larger than the runoff ratio, indicating the underproduce of the runoff volume from rainfall. This disproportionate transfer of the rainfall to runoff volume is also reported by NOAA's National Water Model (Viterbo *et al.*, 2020). In our study this bias of runoff production likely sources from the calibration process, where calibrated runoff volume is still smaller than the observation (Table 6, Exp. Cal). Thus, the amount of rainfall volume required to generate observed runoff may need to be higher than the actual value. Here, we name this amount of rainfall as “model true”.

The runoff-to-rainfall ratio is the runoff volume divided by the corresponding rainfall volume, which can be used to indicate the partition between rainfall to runoff and to measure the flooding tendency. Among the one-way coupled WRF-Hydro simulations, we found that the runoff-to-rainfall ratio gets larger as the simulated rainfall volume increases. This is reasonable since the soil deficit is relatively constant and higher percent of rainfall would be partitioned into runoff as the soil become saturated. In such case, there should be an amplifying effect during the error translation from simulated rainfall input to the runoff volume output if the former is larger than the “model true”. That is, the ratio of the modeled runoff volume bias to that of rainfall volume is likely to increase as overestimation in simulated rainfall gets more significant. On the contrary, if the rainfall amount is underestimated compared to the “model true” in a series of one-way coupled applications, the negative bias with the simulated runoff volume driven by rainfall input with significant negative bias will be disproportionately low.

The bias of peak discharge in general follows that of runoff volume. This indicates the control the runoff volume on the magnitude of peak flow. In addition, we apply the ratio between runoff volume to peak discharge (VP ratio) to investigate the flood tendency to occur over the basins. Smaller VP ratio indicates larger partition of runoff volume to peak discharge, indicating higher peak flow tendency. Among the three one-way coupled simulations over each basin, the VP ratio generally decreases with increasing runoff. Thus, larger amount of rainfall volume will be likely to result in disproportionately higher peak flow in simulation. In this case, considering the amplifying effect of the positive bias from rainfall volume to runoff volume, the simulated peak flow is expected to be further overestimated under such condition. On the other hand, if the runoff is underestimated due to the underestimation in rainfall, the simulated peak discharge will be even smaller than actual. This suggests that if the calibrated runoff is less than observed, as the positive bias of the simulated rainfall volume get larger, the one-way coupled WRF-Hydro tends to provide disproportionately higher than actual peak discharge. Meanwhile, the less than "model true" rainfall is likely to provide much lower-than-actual peak discharge, resulting in the miss of flood signal.

Timing is another important variable in flood forecasting. Here, the timing signature of the flood response simulation and its relation to rainfall input is investigated with the time of peak discharge and rainfall centroid. For the one-way coupled WRF-Hydro simulation, the modeled peak discharge tends to appear earlier than the observation, which can be a result of the errors in calibration process where the calibrated timing of peak is earlier than observation (Table 6, Exp. Cal). In addition, simulated rainfall centroid from WRF also shows an early rainfall signal. These two factors determined most the timing error of simulated peak discharge. An accurate forecast of the timing character of hurricane induced rainfall is still challenging. One possible solution of decreasing the timing error of the simulated peak discharge is to reduce the timing bias inherited from the model calibration process.

5. Summary and Conclusion

This study examines the performance of WRF-Hydro, a fully distributed and processed based hydrometeorological system, in simulating flood response during hurricane Florence over the Cape Fear River basin. The examination was carried out on WRF-Hydro in both offline and one-way coupled mode.

In offline mode, we focus on the evaluation on the model's strength and limitation in capturing the spatially varied flood response over a coastal watershed that is influenced by complex factors including water management, flood plain attenuation, land cover and channel roughness variation. As a grid-based hydrometeorological modeling system, WRF-Hydro has the potential to satisfactorily capture the flood response at multiple scales. However, to achieve that, improvement in model algorithm to support grid-based or sub-basin wise channel parameters, to represent overbank flow and flood plain attenuation effect, as well as water management influence is needed. As demonstrated in this study, driven by NLDAS2 and Stage IV, the calibrated WRF-Hydro is at least able to reproduce the flood response with satisfactory accuracy at sub-basin scale as long as the meteorological input is accurate, and the spatial heterogeneity of hydrological characters are considered.

In one-way coupled mode, WRF-Hydro system is applied following the sequence that meteorological condition is first produced by the WRF simulation and then used to drive the calibrated hydrological component to simulate the streamflow response as the end-product. Complex error interactions occur during this process and finally present in the simulated streamflow. Due to the model uncertainty involved in rainfall simulation from WRF with any single physical scheme, an ensemble simulation is always recommended to cover the actual flood magnitude. Unfortunately, regardless of the microphysics schemes used, a decent simulation of the temporal variation of hurricane induced rainfall is more challenging than that of the storm total rainfall amount. Nonetheless, the WRF-Hydro system can still provide reasonable flood simulation with the peak flow covered by the results given that flood response of the target basin is controlled by rainfall total rather than rainfall intensity.

The calibrated WRF-Hydro model used in one-way coupled model is from the offline calibration. During calibration, the model parameters are adjusted to the end of an optimal model performance judged by the selected objective function. During this process, there is always a trade-off between timing and amplitude error/similarity. In this case, neither timing nor amplitude can be perfectly matched. The bias in timing or magnitude will then be propagated into the one-way coupled simulation. In our study, a general under-reproduce of runoff and faster response of watershed is associated with the calibration process, which is also reported by NOAA's National Water Model (Viterbo *et al.*, 2020). Due to the under-produce of runoff, there should be a "model true" rainfall total to generate the runoff volume that is perfectly agreed with the observation at a gauge station. For the applications of WRF-Hydro system with one-way coupled mode in which the rainfall total is overestimated compared to the "model true", larger positive bias in rainfall will be likely to induce disproportionately higher runoff volume and even larger peak flood. Thus, when underproduction of runoff volume occurred with calibration, peak flow simulation from WRF-Hydro system in one-way coupled mode tends to be more conservative with the increasing overestimate in rainfall input. On the contrary, caution should be taken if considerable underestimate exists with the rainfall simulation since the peak flow will be disproportionately underestimated. In addition, the timing error with the streamflow response seems to be dominated by the timing bias associated with calibration and that sourced from the rainfall input. Given the propagation of both timing and amplitude errors from offline calibration to the following streamflow simulation in one-way coupled mode, two extra benchmark calibrations are recommended. In each of the calibration, objective function can be selected to weight more on perfect match in timing or amplitude rather than a balance between the two.

Data Availability Statement

The data that support the findings of this study are available from the corresponding author upon reasonable request.

References

Alford JB, Debbage KG, Mallin MA, Liu ZJ. 2016. Surface water quality and landscape gradients in the north carolina cape fear river basin: The key role of fecal coliform. *Southeastern Geographer* **56** (4): 428–453 DOI: 10.1353/sgo.2016.0045

Bowman AL, Franz KJ, Hogue TS, Kinoshita AM. 2015. MODIS-Based Potential Evapotranspiration Demand Curves for the Sacramento Soil Moisture Accounting Model DOI: 10.1061/(ASCE)

Cai X, Yang ZL, David CH, Niu GY, Rodell M. 2014. Hydrological evaluation of the noah-MP land surface model for the Mississippi River Basin. *Journal of Geophysical Research* **119** (1): 23–38 DOI: 10.1002/2013JD020792

Curtis Weaver BJ, Pope Raleigh BF, Carolina N. 2001. Low-Flow Characteristics and Discharge Profiles for Selected Streams in the Available at: http://nc.water.usgs.gov. [Accessed 21 March 2020]

Dinan T. 2017. Projected Increases in Hurricane Damage in the United States: The Role of Climate Change and Coastal Development. *Ecological Economics* **138**: 186–198 DOI: 10.1016/j.ecolecon.2017.03.034

Feaster TD, Weaver JC, Gotvald AJ, Kolb KR. 2018. Preliminary peak stage and streamflow data for selected U.S. Geological Survey streamgaging stations in North and South Carolina for flooding following Hurricane Florence, September 2018. *Open-File Report 2018-1172* (October) DOI: 10.3133/ofr20181172

Fersch B, Senatore A, Adler B, Arnault J, Mauder M, Schneider K, Völksch I, Kunstmann H. 2020. High-resolution fully coupled atmospheric–hydrological modeling: a cross-compartment regional water and energy cycle evaluation. *Hydrology and Earth System Sciences* **24** (5): 2457–2481 DOI: 10.5194/hess-24-2457-2020

Gochis DJ, Barlage M, Cabell R, Casali M, Dugger A, FitzGerald K, McAllister M, McCreight J, RafieeiNasab A, Read L, et al. 2020. The WRF-Hydro modeling system technical description, (Version 5.1.1). *NCAR Technical Note*: 107 Available at: https://ral.ucar.edu/sites/default/files/public/projects/wrf_hydro/technical-description-user-guide/wrf-hydro-v5.1.1-technical-description.pdf

Hamel P, Guswa AJ. 2015. Uncertainty analysis of a spatially explicit annual water-balance model: Case study of the Cape Fear basin, North Carolina. *Hydrology and Earth System*

Sciences **19** (2): 839–853 DOI: 10.5194/hess-19-839-2015

Hong S, Lim K, Kim J, Lim JJ, Dudhia J. 2005. WRF Single-Moment 6-Class Microphysics Scheme (WSM6): 5–6

Hong SY, Noh Y, Dudhia J. 2006. A new vertical diffusion package with an explicit treatment of entrainment processes. *Monthly Weather Review* **134** (9): 2318–2341 DOI: 10.1175/MWR3199.1

Iacono MJ, Delamere JS, Mlawer EJ, Shephard MW, Clough SA, Collins WD. 2008. Radiative forcing by long-lived greenhouse gases: Calculations with the AER radiative transfer models. *Journal of Geophysical Research Atmospheres* **113** (13): 2–9 DOI: 10.1029/2008JD009944

Kerandi N, Arnault J, Laux P, Wagner S, Kitheka J, Kunstmann H. 2018. Joint atmospheric-terrestrial water balances for East Africa: a WRF-Hydro case study for the upper Tana River basin. *Theoretical and Applied Climatology* **131** (3–4): 1337–1355 DOI: 10.1007/s00704-017-2050-8

Knutson TR, McBride JL, Chan J, Emanuel K, Holland G, Landsea C, Held I, Kossin JP, Srivastava AK, Sugi M. 2010. Tropical cyclones and climate change. *Nature Geoscience* **3** (3): 157–163 DOI: 10.1038/ngeo779

Li L, Gochis DJ, Sobolowski S, Mesquita MDS. 2017. Evaluating the present annual water budget of a Himalayan headwater river basin using a high-resolution atmosphere-hydrology model. *Journal of Geophysical Research* **122** (9): 4786–4807 DOI: 10.1002/2016JD026279

Li L, Pontoppidan M, Sobolowski S, Senatore A. 2020. The impact of initial conditions on convection-permitting simulations of a flood event over complex mountainous terrain. *Hydrology and Earth System Sciences* **24** (2): 771–791 DOI: 10.5194/hess-24-771-2020

Lin P, Hopper LJ, Yang Z-L, Lenz M, Zeitler JW. 2018a. Insights into Hydrometeorological Factors Constraining Flood Prediction Skill during the May and October 2015 Texas Hill Country Flood Events. *Journal of Hydrometeorology* **19** (8): 1339–1361 DOI: 10.1175/jhm-d-18-0038.1

Lin P, Hopper LJ, Yang ZL, Lenz M, Zeitler JW. 2018b. Insights into hydrometeorological factors constraining flood prediction skill during the May and October 2015 Texas Hill Country flood events. *Journal of Hydrometeorology* **19** (8): 1339–1361 DOI: 10.1175/JHM-D-18-0038.1

Lin P, Rajib MA, Yang ZL, Somos-Valenzuela M, Merwade V, Maidment DR, Wang Y, Chen L. 2018c. Spatiotemporal Evaluation of Simulated Evapotranspiration and Streamflow over Texas Using the WRF-Hydro-RAPID Modeling Framework. *Journal of the American Water Resources Association* **54** (1): 40–54 DOI: 10.1111/1752-1688.12585

Lin Y. 2011. GCIP/EOP Surface: Precipitation NCEP/EMC 4KM Gridded Data (GRIB) Stage IV Data. Version 1.0. DOI: https://doi.org/10.5065/D6PG1QDD.

Long D, Longuevergne L, Scanlon BR. 2014. Uncertainty in evapotranspiration from land surface modeling, remote sensing, and GRACE satellites. *Water Resources Research* **50** (2): 1131–1151 DOI: 10.1002/2013WR014581

Miller DA, White RA. 1998. A Conterminous United States Multilayer Soil Characteristics Dataset for Regional Climate and Hydrology Modeling. *Earth Interactions* **2** (1): 2–2 DOI: 10.1175/1087-3562(1998)002<0002:cusms>2.0.co;2

Mitchell KE, Lohmann D, Houser PR, Wood EF, Schaake JC, Robock A, Cosgrove BA, Sheffield J, Duan Q, Luo L, et al. 2004. The multi-institution North American Land Data Assimilation System (NLDAS): Utilizing multiple GCIP products and partners in a continental distributed hydrological modeling system. *Journal of Geophysical Research D: Atmospheres* **109** (7): 1–32 DOI: 10.1029/2003jd003823

Morrison H, Thompson G, Tatarskii V. 2009. Impact of cloud microphysics on the development of trailing stratiform precipitation in a simulated squall line: Comparison of one- and two-moment schemes. *Monthly Weather Review* **137** (3): 991–1007 DOI: 10.1175/2008MWR2556.1

Mu Q, Zhao M, Running SW. 2011. Improvements to a MODIS global terrestrial evapotranspiration algorithm. *Remote Sensing of Environment* **115** (8): 1781–1800 DOI: 10.1016/j.rse.2011.02.019

Niu GY, Yang ZL, Mitchell KE, Chen F, Ek MB, Barlage M, Kumar A, Manning K, Niyogi D, Rosero E, et al. 2011a. The community Noah land surface model with multiparameterization options (Noah-MP): 1. Model description and evaluation with local-scale measurements. *Journal of Geophysical Research Atmospheres* **116** (12): 1–19 DOI: 10.1029/2010JD015139

Niu GY, Yang ZL, Mitchell KE, Chen F, Ek MB, Barlage M, Kumar A, Manning K, Niyogi D, Rosero E, et al. 2011b. The community Noah land surface model with multiparameterization options (Noah-MP): 1. Model description and evaluation with local-scale measurements. *Journal of Geophysical Research Atmospheres* **116** (12) DOI: 10.1029/2010JD015139

Papaioannou G, Varlas G, Terti G, Papadopoulos A, Loukas A, Panagopoulos Y, Dimitriou E. 2019. Flood inundation mapping at ungauged basins using coupled hydrometeorological-hydraulic modelling: The catastrophic case of the 2006 Flash Flood in Volos City, Greece. *Water (Switzerland)* **11** (11): 1–28 DOI: 10.3390/w11112328

Parajuli PB, Jayakody P, Ouyang Y. 2018. Evaluation of Using Remote Sensing Evapotranspiration Data in SWAT. *Water Resources Management* **32** (3): 985–996 DOI: 10.1007/s11269-017-1850-z

Rappaport EN. 2014. Fatalities in the United States from Atlantic Tropical Cyclones: New Data and Interpretation. *Bulletin of the American Meteorological Society* **95** (3): 341–346 DOI: 10.1175/BAMS-D-12-00074.1

Rummler T, Arnault J, Gochis D, Kunstmann H. 2019. Role of Lateral Terrestrial Water Flow on the Regional Water Cycle in a Complex Terrain Region: Investigation With a Fully Coupled Model System. *Journal of Geophysical Research: Atmospheres* **124** (2): 507–529 DOI: 10.1029/2018JD029004

Running SW, Mu Q, Zhao M. MOD16A2 MODIS/Terra Net Evapotranspiration 8-Day L4 Global 500m SIN Grid V006 [Data set]. *NASA EOSDIS Land Processes DAAC* Available at: https://doi.org/10.5067/MODIS/MOD16A2.006 [Accessed 23 January 2021]

Ryu Y, Lim YJ, Ji HS, Park HH, Chang EC, Kim BJ. 2017. Applying a coupled hydrometeorological simulation system to flash flood forecasting over the Korean Peninsula. *Asia-Pacific Journal of Atmospheric Sciences* **53** (4): 421–430 DOI: 10.1007/s13143-017-0045-0

Senatore A, Davolio S, Furnari L, Mendicino G. 2020a. Reconstructing flood events in mediterranean coastal areas using different reanalyses and high-resolution meteorological models. *Journal of Hydrometeorology* **21** (8): 1865–1887 DOI: 10.1175/JHM-D-19-0270.1

Senatore A, Furnari L, Mendicino G. 2020b. Impact of high-resolution sea surface temperature representation on the forecast of small Mediterranean catchments' hydrological responses to heavy precipitation. *Hydrology and Earth System Sciences* **24** (1): 269–291 DOI: 10.5194/hess-24-269-2020

Senatore A, Mendicino G, Gochis DJ, Yu W, Yates DN, Kunstmann H. 2015. Fully coupled atmosphere-hydrology simulations for the central Mediterranean: Impact of enhanced hydrological parameterization for short and long time scales. *Journal of Advances in Modeling Earth Systems* **7** (4): 1693–1715 DOI: 10.1002/2015MS000510

Smith JA, Baeck ML, Villarini G, Krajewski WF. 2010. The hydrology and hydrometeorology of flooding in the Delaware River basin. *Journal of Hydrometeorology* **11** (4): 841–859 DOI: 10.1175/2010JHM1236.1

Somos-Valenzuela MA, Palmer RN. 2018. Use of WRF-hydro over the Northeast of the US to estimate water budget tendencies in small watersheds. *Water (Switzerland)* **10** (12) DOI: 10.3390/w10121709

Thompson G, Field PR, Rasmussen RM, Hall WD. 2008. Explicit forecasts of winter precipitation using an improved bulk microphysics scheme. Part II: Implementation of a new snow parameterization. *Monthly Weather Review* **136** (12): 5095–5115 DOI: 10.1175/2008MWR2387.1

Tolson BA, Shoemaker CA. 2007. Dynamically dimensioned search algorithm for computationally efficient watershed model calibration. *Water Resources Research* **43** (1): 1–16 DOI: 10.1029/2005WR004723

Verri G, Pinardi N, Gochis D, Tribbia J, Navarra A, Coppini G, Vukicevic T. 2017. A meteo-hydrological modelling system for the reconstruction of river runoff: The case of the Ofanto river catchment. *Natural Hazards and Earth System Sciences* **17** (10): 1741–1761 DOI: 10.5194/nhess-17-1741-2017

Villarini G, Smith JA. 2010. Flood peak distributions for the eastern United States. *Water Resources Research* **46** (6) DOI: 10.1029/2009WR008395

Viterbo F, Mahoney K, Read L, Salas F, Bates B, Elliott J, Cosgrove B, Dugger A, Gochis D, Cifelli R. 2020. A multiscale, hydrometeorological forecast evaluation of national water model forecasts of the may 2018 Ellicott City, Maryland, Flood. *Journal of Hydrometeorology* **21** (3): 475–499 DOI: 10.1175/JHM-D-19-0125.1

Walsh KJE, McBride JL, Klotzbach PJ, Balachandran S, Camargo SJ, Holland G, Knutson TR, Kossin JP, Lee T, Sobel A, et al. 2016. Tropical cyclones and climate change. *Wiley Interdisciplinary Reviews: Climate Change* **7** (1): 65–89 DOI: 10.1002/wcc.371

Weaver JC, Carolina N. 1997. Low-Flow Characteristics and Profiles for the Deep River in the

Cape Fear River Basin, North Carolina Division of Water Quality and Division of Water Resources of the

Wing OEJ, Bates PD, Smith AM, Sampson CC, Johnson KA, Fargione J, Morefield P. 2018. Estimates of present and future flood risk in the conterminous United States. *Environmental Research Letters* **13** (3) DOI: 10.1088/1748-9326/aaac65

Xia Y, Mitchell K, Ek M, Sheffield J, Cosgrove B, Wood E, Luo L, Alonge C, Wei H, Meng J, et al. 2012. Continental-scale water and energy flux analysis and validation for the North American Land Data Assimilation System project phase 2 (NLDAS-2): 1. Intercomparison and application of model products. *Journal of Geophysical Research Atmospheres* **117** (3) DOI: 10.1029/2011JD016048

Xue Z, Gochis D, Yu W, Keim B, Rohli R, Zang Z, Sampson K, Dugger A, Sathiaraj D, Ge Q. 2018. Modeling Hydroclimatic Change in Southwest Louisiana Rivers. *Water* **10** (5): 596 DOI: 10.3390/w10050596

Yin D, Xue ZG, Gochis DJ, Yu W, Morales M. 2020. A Process-Based , Fully Distributed Soil Erosion and Sediment Transport Model for WRF-Hydro

Yucel I, Onen A, Yilmaz KK, Gochis DJ. 2015. Calibration and evaluation of a flood forecasting system: Utility of numerical weather prediction model, data assimilation and satellite-based rainfall. *Journal of Hydrology* **523**: 49–66 DOI: 10.1016/j.jhydrol.2015.01.042

Zhang J, Lin P, Gao S, Fang Z. 2020. Understanding the re-infiltration process to simulating streamflow in North Central Texas using the WRF-hydro modeling system. *Journal of Hydrology* **587**: 124902 DOI: 10.1016/j.jhydrol.2020.124902

Table 1. Setup and configuration of the numerical experiments

Exp.	Initial and boundary condition	Microphysics scheme		Simulation period
		WRFD01	WRFD02	
OFF1	ERA5	WSM 6	WSM 6	1800 UTC 13 Sep. – 0600 UTC 18 Sep.2018
OFF2		Thompson	Thompson	
OFF3		Morrison	Morrison	

Table 2. Overview of the calibration methodology

River	USGS Gage Name	USGS Gage Identification Number	Drainage area (km^2)	Calibration Period	Calibration method
Haw River	Bynum	02096960	3302	UTC 0000 14 - UTC 0000 24 September	Automatic with NCAR calibration tool
Deep River	Moncure	02102000	3714		
Little River	Manchester	02103000	901		Manually with a stepwise method
Black River	Tomahawk	02106500	1751		
Northeast Cape Fear River	Chinquapin	02108000	1551		
Cape Fear River	Kelly	02105769	13610	UTC 0000 14 - UTC 0000 30 September	

Table 3. Parameters selected for calibration over the Haw River basin

Parameters	Minimum value	Maximum value	Physical meaning
refkdt	0.1	3	A tunable parameter that is used to calculate the surface infiltration.
slope	0	1	A scaling parameter that is used to calculate the recharge from soil column to underlying aquifer in land surface model.
LKSATFAC	10	10000	A scaling parameter used to adjust the saturated hydraulic conductivity of soil
OVROUGHRTFAC	0.01	100000	A scaling parameter used to adjust the overland surface roughness.

Table 4 MODIS and Model Simulated ET

ET (mm)	Haw River basin	Deep River basin	Little River basin	Black River basin	NE CFR basin	Cape Fear River basin
MODIS	48.3	51.4	50.1	50.3	49.9	50.2
Model	46.3	57.1	57.4	49.3	51.3	55.1

Table 5. Statistical performance of WRF simulation in producing hourly areal rainfall rate

Basin	Exp.	Bias (mm/h)	RMSE (mm/h)	R^2	NSE
Haw River (02096960)	OFF1	1.40	3.6	0.34	-1.43
	OFF2	0.13	2.8	0.02	-0.45
	OFF3	0.34	2.3	0.25	-0.05
Deep River (02102000)	OFF1	0.37	3.4	0.27	-0.09
	OFF2	-0.84	3.2	0.13	0.04
	OFF3	-0.57	2.9	0.28	0.20
Little River (02103000)	OFF1	1.51	5.6	0.08	-2.36
	OFF2	-0.72	3.3	0.10	-0.20
	OFF3	-0.90	3.0	0.21	0.02
Black River (02106500)	OFF1	-0.07	5.8	0.04	-0.74
	OFF2	-1.16	5.2	0.05	-0.44
	OFF3	-1.73	5.7	0.03	-0.69
NE CFR (02108000)	OFF1	-0.70	7.1	0.09	-0.59
	OFF2	-1.96	6.5	0.07	-0.35
	OFF3	-2.35	7.1	0.04	-0.60
Cape Fear River (02105769)	OFF1	0.87	2.0	0.56	0.06
	OFF2	-0.69	2.1	0.12	-0.07
	OFF3	-0.67	1.7	0.46	0.35

Table 6. Model performance over Cape Fear River and its major tributaries in one-way coupled mode

Basin	Exp.	Stage IV Rainfall (mm)	Obs. Runoff (mm)	Obs. Peak Discharge (m^3/s)	NSE	Rainfall ratio	Runoff ratio	Runoff to Rainfall ratio	Peak discharge ratio	Runoff To Peak Discharge Ratio (h)	Rainfall Centroid difference (hour)	Peak Timing Difference (hour)
Haw River (02096960)	OFF 1	122	81	1486	-1.15	2.11	1.92	0.58	2.67	34	5	12
	OFF 2				0.28	1.11	0.56	0.33	0.36	67	30	45
	OFF 3				0.77	1.27	0.83	0.41	1.33	31	-1	2
	Cal				0.91	1	0.72	0.46	0.84	41	0	0.15
Deep River (02102000)	OFF 1	224	170	1820	0.64	1.16	0.91	0.55	1.71	49	4	8
	OFF 2				-0.28	0.64	0.30	0.36	0.30	92	19	5
	OFF 3				0.25	0.76	0.48	0.44	0.57	74	-2	3
	Cal				0.84	1	0.87	0.63	1.30	62	0	4
Little River (02103000)	OFF 1	269	170	496	-0.57	1.54	1.62	0.62	1.73	74	1	15
	OFF 2				0.18	0.74	0.50	0.41	0.38	97	0	1
	OFF 3				-0.14	0.68	0.40	0.33	0.28	104	-11	-12
	Cal				0.80	1	0.99	0.57	0.87	88	0	4
Black River (02106500)	OFF 1	411	301	1559	0.67	0.98	0.86	0.58	0.63	124	11	18
	OFF 2				0.39	0.73	0.55	0.53	0.37	119	13	30
	OFF 3				0.04	0.59	0.41	0.46	0.30	119	19	40
	Cal				0.98	1	0.97	0.66	0.94	90	0	4
NE CFR (02108000)	OFF 1	512	334	1163	0.69	0.87	0.96	0.65	1.28	86	13	15
	OFF 2				0.63	0.63	0.61	0.62	0.62	118	13	10
	OFF 3				0.62	0.56	0.52	0.53	0.57	100	16	22
	Cal				0.79	1	1.21	0.74	1.60	88	0	9
Cape Fear River (02105769)	OFF 1	237	134	2215	-0.36	1.35	1.10	0.48	2.19	114	7	23
	OFF 2				-0.16	0.72	0.50	0.40	0.55	191	20	2
	OFF 3				-0.04	0.73	0.50	0.40	0.60	191	3	-5
	Cal				0.42	2.11	0.99	0.56	1.71	132	0	18

a: For reference, calibrated model performance (Exp. Cal) is also provided.

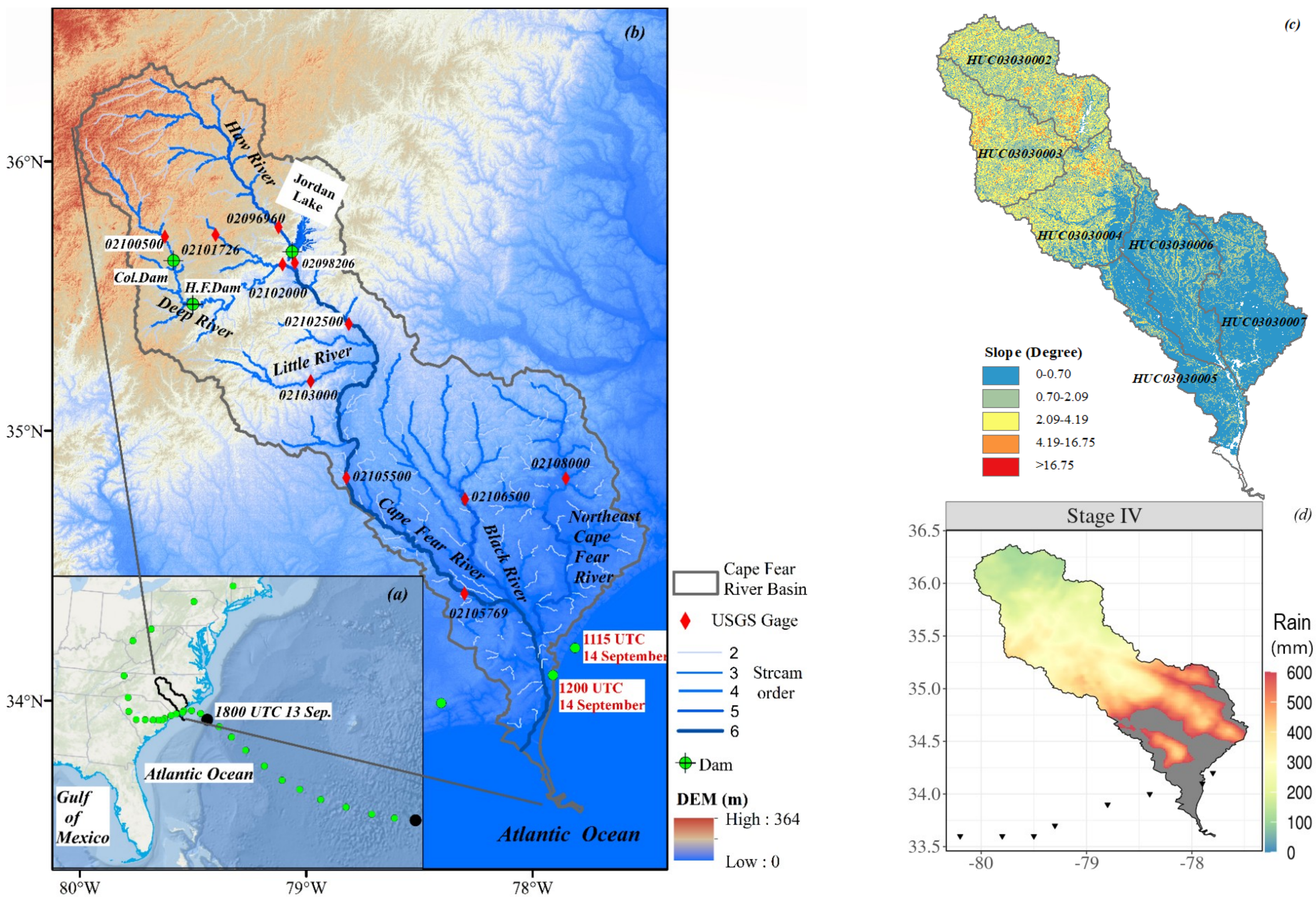

Figure 1. (a) NOAA best track for Hurricane Florence with 6 hours interval. The Cape Fear River basin is outlined with soil black line. (b) Topography and river network, 11 USGS gages, Coleridge Dam (Col. Dam), High Falls Dam (H.F. Dam) and Jordan Lake Dam in WRF-Hydro domain (WHD01). The NOAA best track for Hurricane Florence with 6 hours interval is also presented with solid green circles. (c) Topographic Slope across the Cape Fear River basin in degree. USGS HUC 8 watersheds are outlined with solid grey line.

(d) Storm total rainfall during 0000 UTC 14 to 0000 UTC 18 September based on Stage IV. The track of hurricane is represented with black triangles.

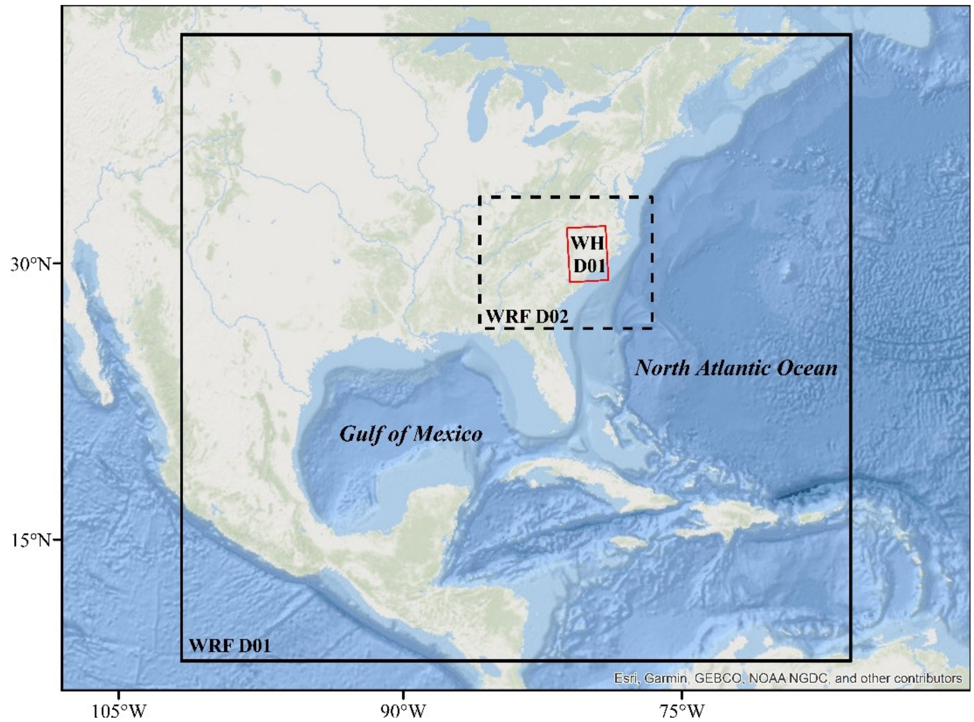

Figure 2. Model domains: the outer domain of WRF (WRF D01, solid black line), the inner domain of WRF (WRF D02, dashed black line) and the domain of WRF_Hydro (WH D01, solid red line).

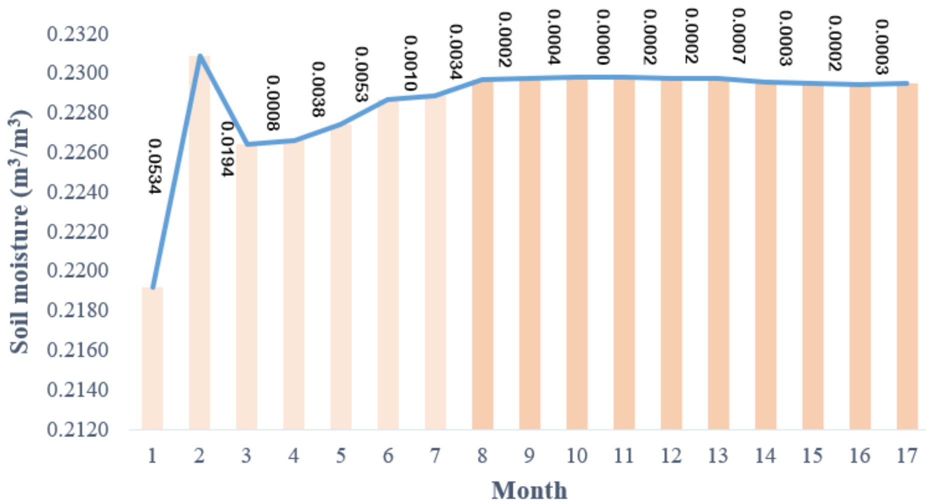

Figure 3. Column averaged soil moisture (m^3/m^3, column bars) over the Cape Fear River basin from numerical experiments with different spin-up time (x axis, unit in month) and its trend line (solid blue line). The relative difference ($|Var^{N+1} - Var^{N}|, Eq.(1)$) is annotated. For the sake of differentiation, column bars of modeling results from experiments with inadequate and adequate spin-up are filled in light and dark orange, respectively.

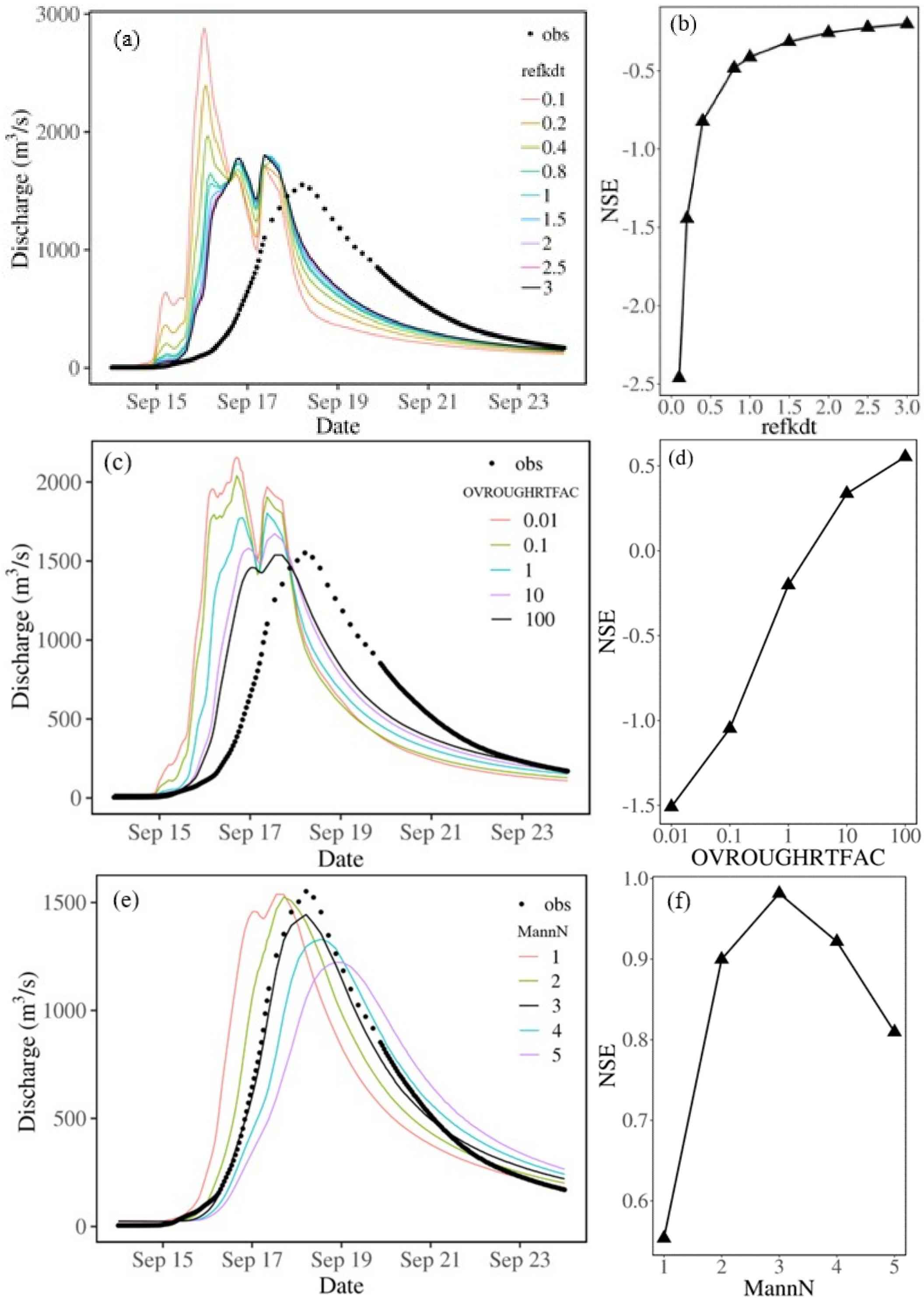

Figure 4. (a) Simulated and observed hydrographs and (b) Model performance (NSE)-*refkdt* relationship over the Black River basin at Tomahawk (USGS gage 02106500) from 9 numerical experiments with various *refkdt* values. (c) and (d):As with a~b, but from five numerical experiments with various *OVROUGHRTFAC* values. (e) and (f): As with a~b, but from five numerical experiments with different *MannN* values. The location of the gage is shown in Figure 1b.

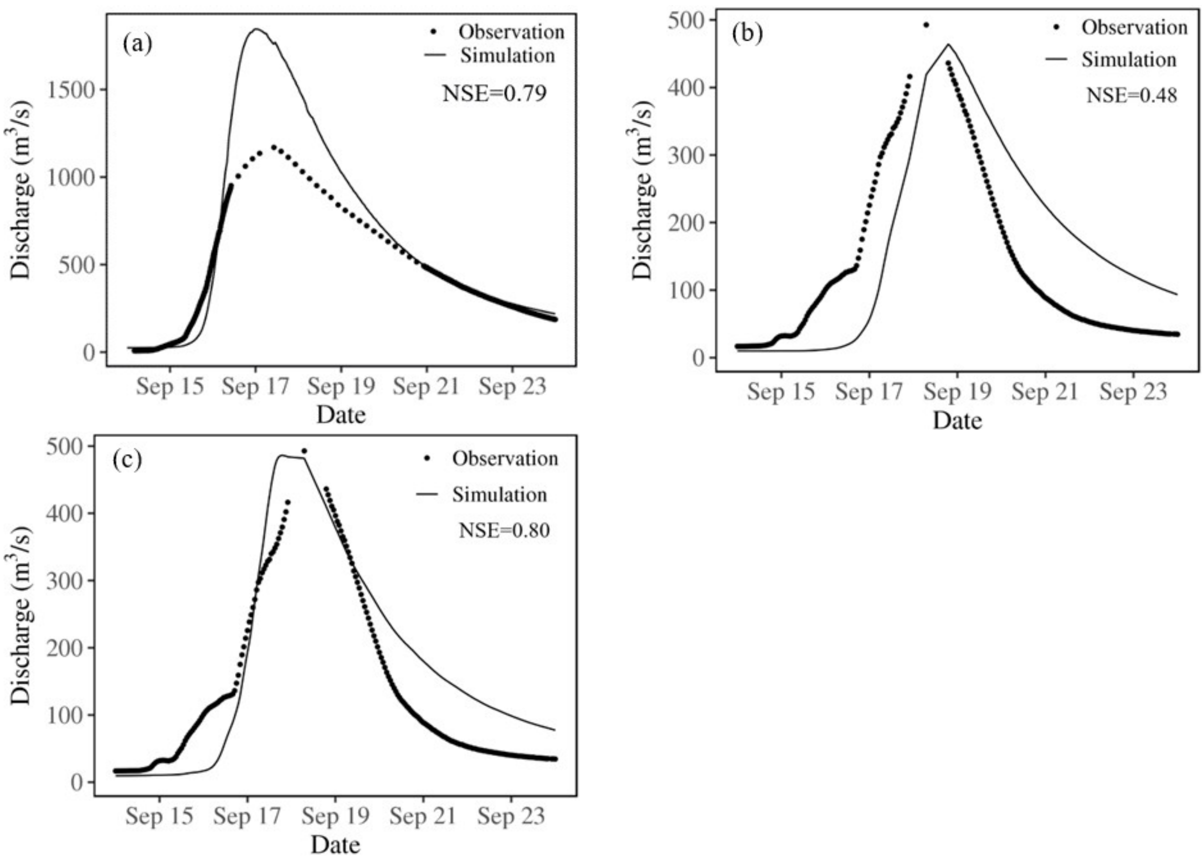

Figure 5. Simulated (solid black line) and observed (black dot) hydrographs for (a): the Northeast Cape Fear River at Chinquapin (USGS gage 02108000), and (b): Little River at Manchester (USGS gage 02103000), respectively, using the calibrated parameters for the Black River basin. (c): Same with (b) but using the recalibrated channel parameters (*MannN*) for the Little River basin. NSE values are also shown.

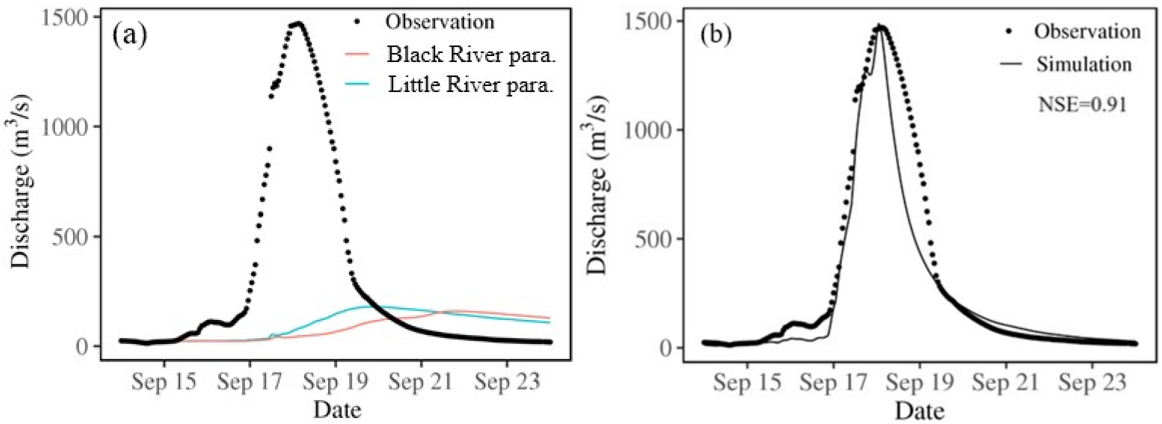

Figure 6. (a) Observed (black dot) and simulated over the Haw River basin at Bynum (USGS gage 02096960) using calibrated parameters for the Black River (red line) and the Little River (blue line). (b) As with a, observed (black dot) and recalibrated hydrographs (solid black line). NSE value is also shown. The location of the gage is shown in Figure 1b.

723

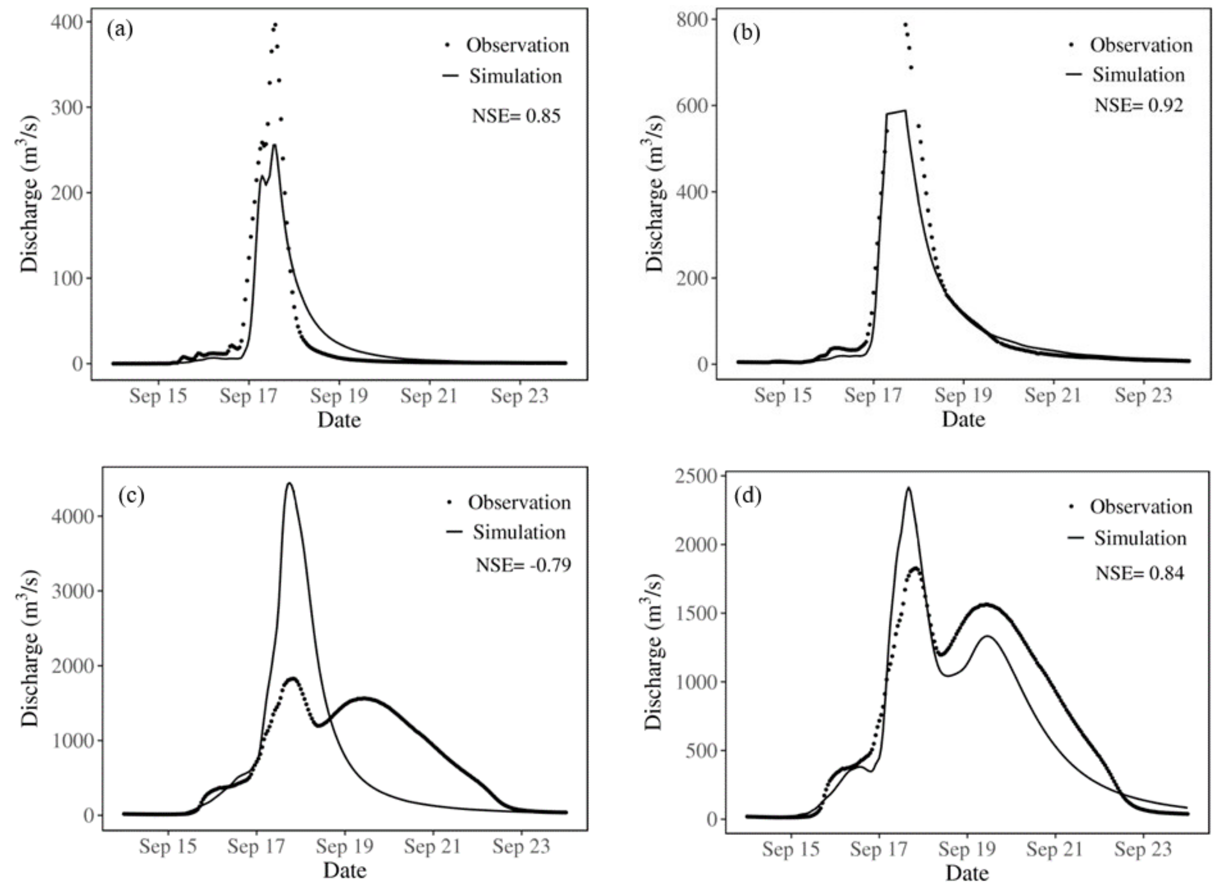

Figure 7. Simulated (solid black line) and observed (black dot) hydrographs for the Deep River basin at (a): Siler City (USGS gage 02101726), (b): Ramseur (USGS gage 02100500) and (c): Moncure (USGS gage 02102000), respectively, using the calibrated parameters for the Haw River basin at Bynum (USGS gage 02096960). (d): Same with (c) but using the recalibrated manning coefficient of channel. NSE values are also shown. The locations of the gages are shown in Figure 1b.

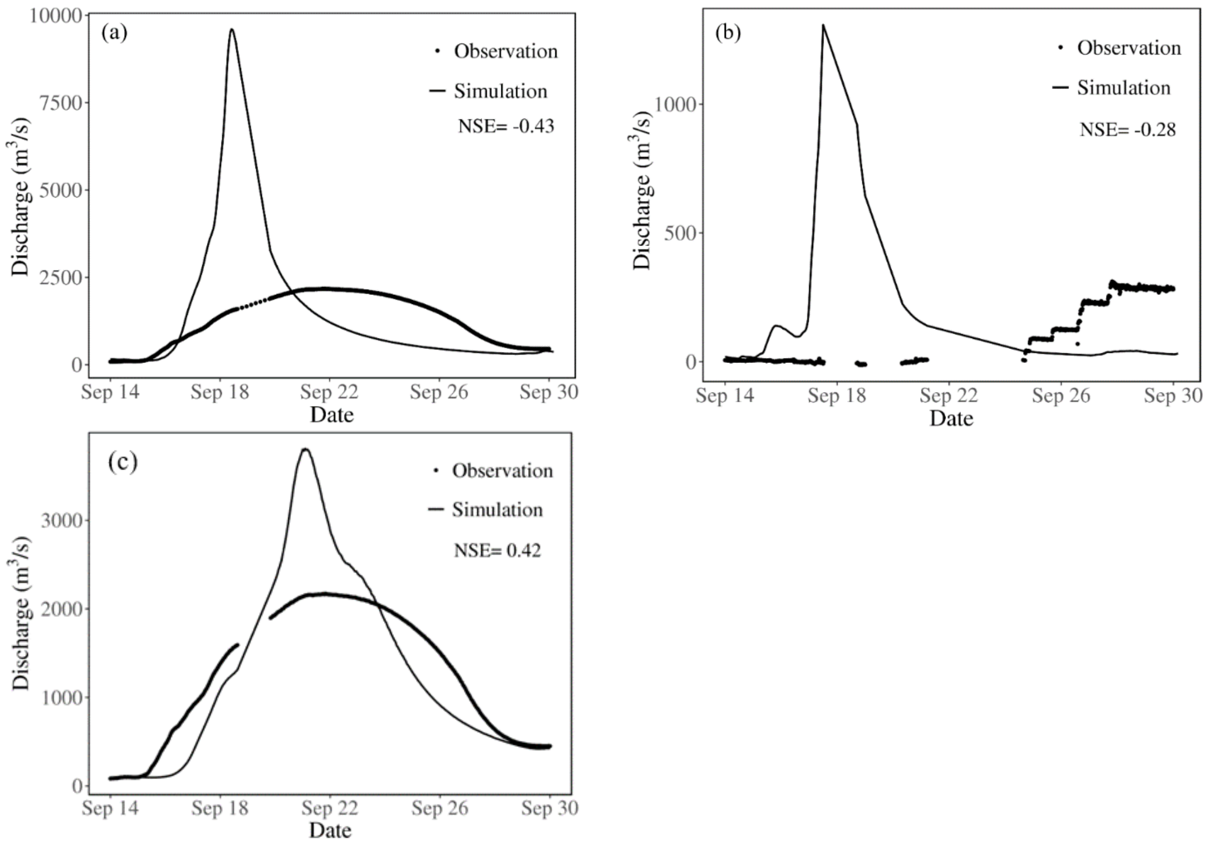

Figure 8. Simulated (solid black line) and observed (black dot) hydrographs for (a) the mainstem of Cape Fear River at Kelly (USGS Gage 02105769) and (b) the outlet of Jordan Lake at Moncure (USGS gage 02098206). (c) Same with (a) but calibrated based on the assimilation of human controlled flow through Jordan Lake Dam at Moncure (USGS gage 02098206). NSE values are also shown. The location of the gage is shown in Figure 1b.

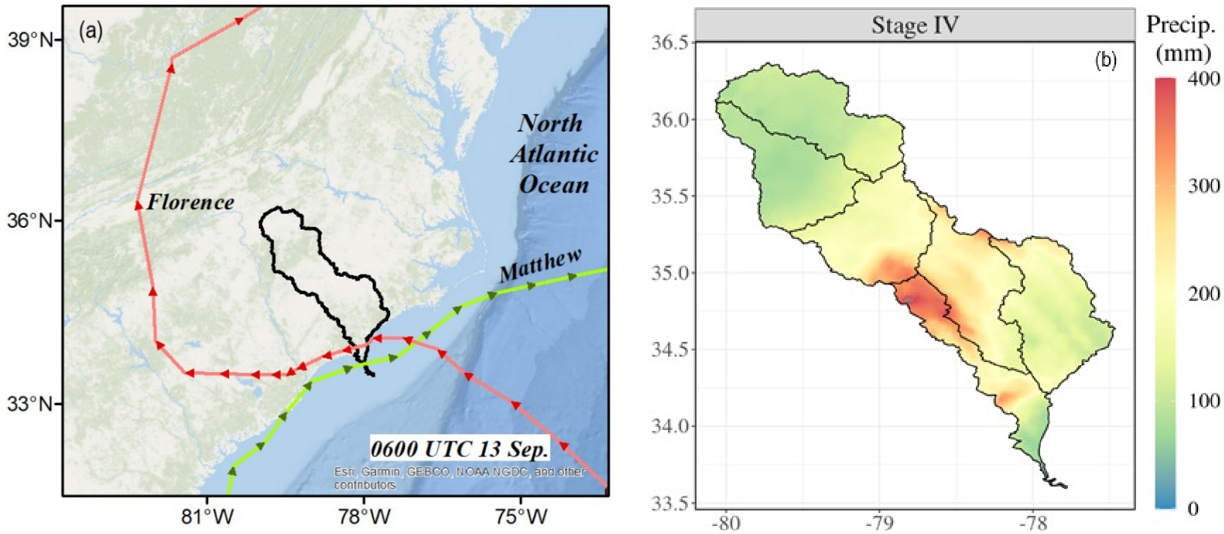

Figure 9. (a) NOAA best track for Hurricane Florence and Matthew with 6 hours interval. CFRB is outlined in solid black line. (b) Accumulative rainfall during 8 to 9 October 2016 over the CFRB associated with Matthew. Rainfall data is from Stage IV.

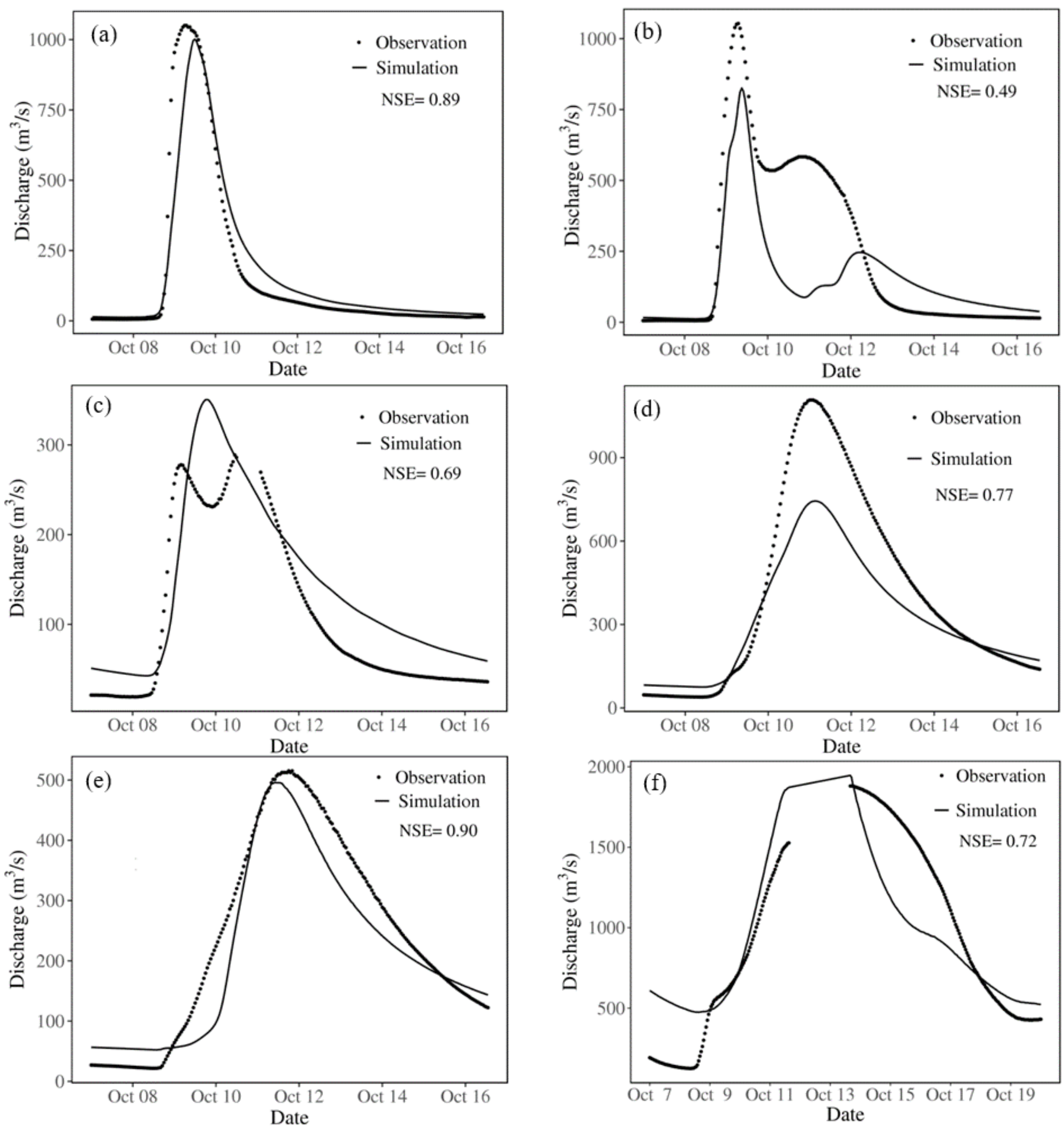

Figure 10. Simulated (solid black line) and observed (black dot) hydrographs for: (a) the Haw River basin at Bynum (USGS gage 02096960), (b) the Deep River basin at Moncure (USGS gage 02102000), (c) the Little River basin at Manchester (USGS gage 02103000), (d) the Black River basin at Tomahawk (USGS gage 02106500), (e) the Northeast Cape Fear River at Chinquapin (USGS gage 02108000) and (f) the mainstem of Cape Fear River at Kelly (USGS gage 02105769). NSE values are also shown. The locations of the gages are shown in Figure 1b.

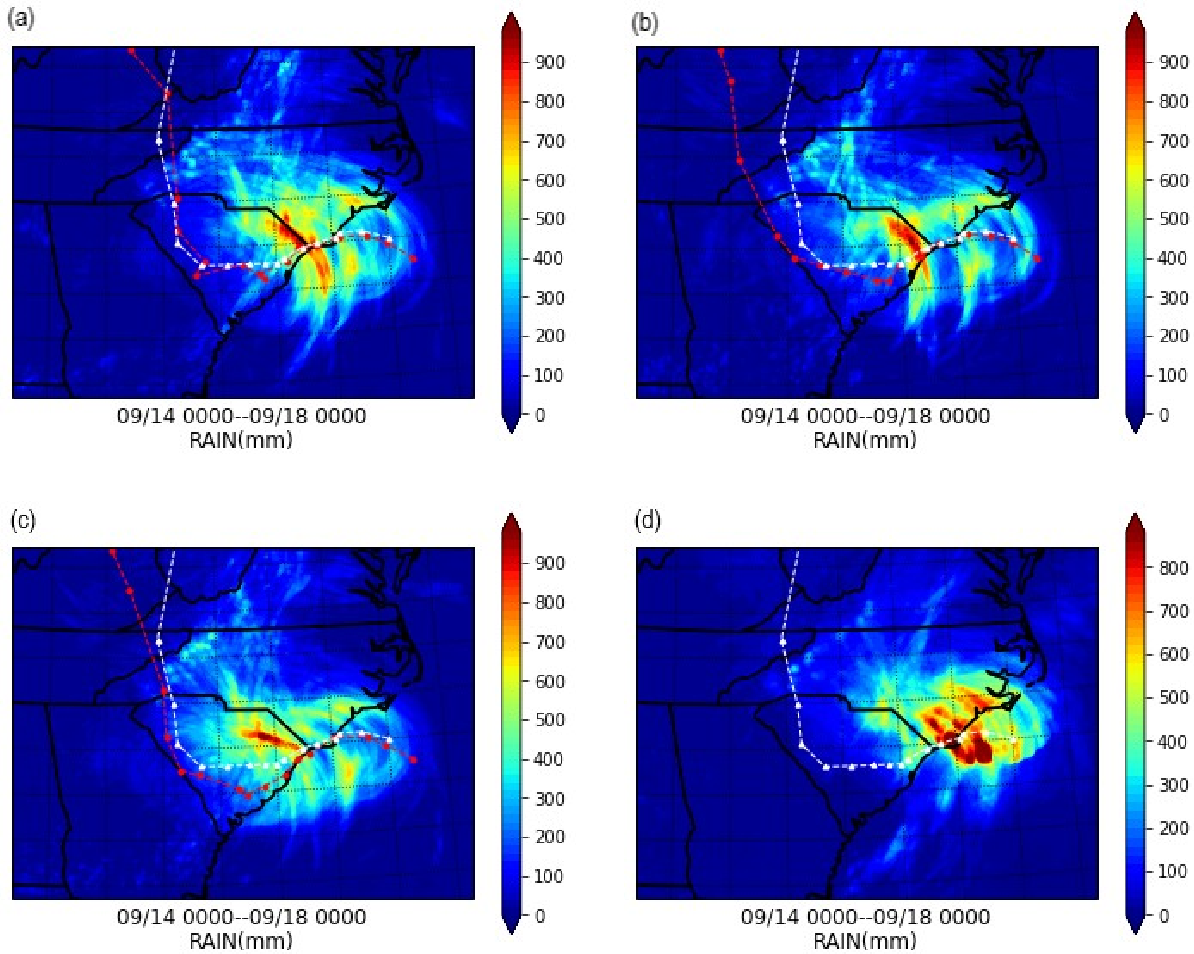

Figure 11. The storm total rainfall during Florence (09/14 0000-09/18 0000 2018) over the inner domain of WRF (WRF D02) from WRF simulation using (a) WSM6 scheme (OFF1), (b) Thompson scheme (OFF2), (c) Morrison scheme (OFF3), and (d) same as a–c, but from Stage IV. The simulated track from each experiment is labeled with red dotted line along with the NOAA best track shown with white dotted line.

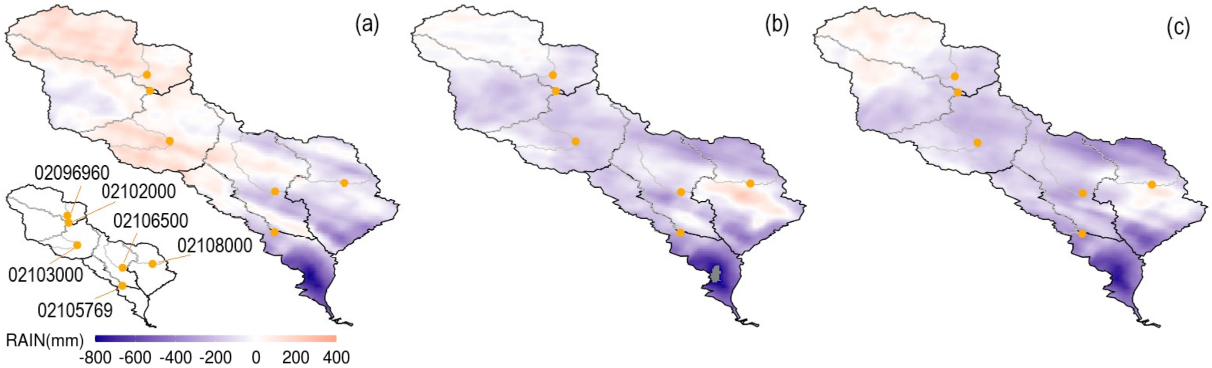

Figure 12. Difference between the storm total rainfall during Florence (09/14 0000-09/18 0000 2018) from Stage IV and that from WRF simulation (Simulation subtracted by Stage IV) with (a)WSM6 scheme (OFF1), (b) Thompson scheme (OFF2) and (c) Morrison scheme (OFF3). The 6 USGS HUC 8 watersheds are outlined in solid black line. The six USGS gages along the main steam of Cape Fear River and its major tributaries (Table 1) and their drainage areas are labeled with solid dots and outlined with solid grey line, respectively.

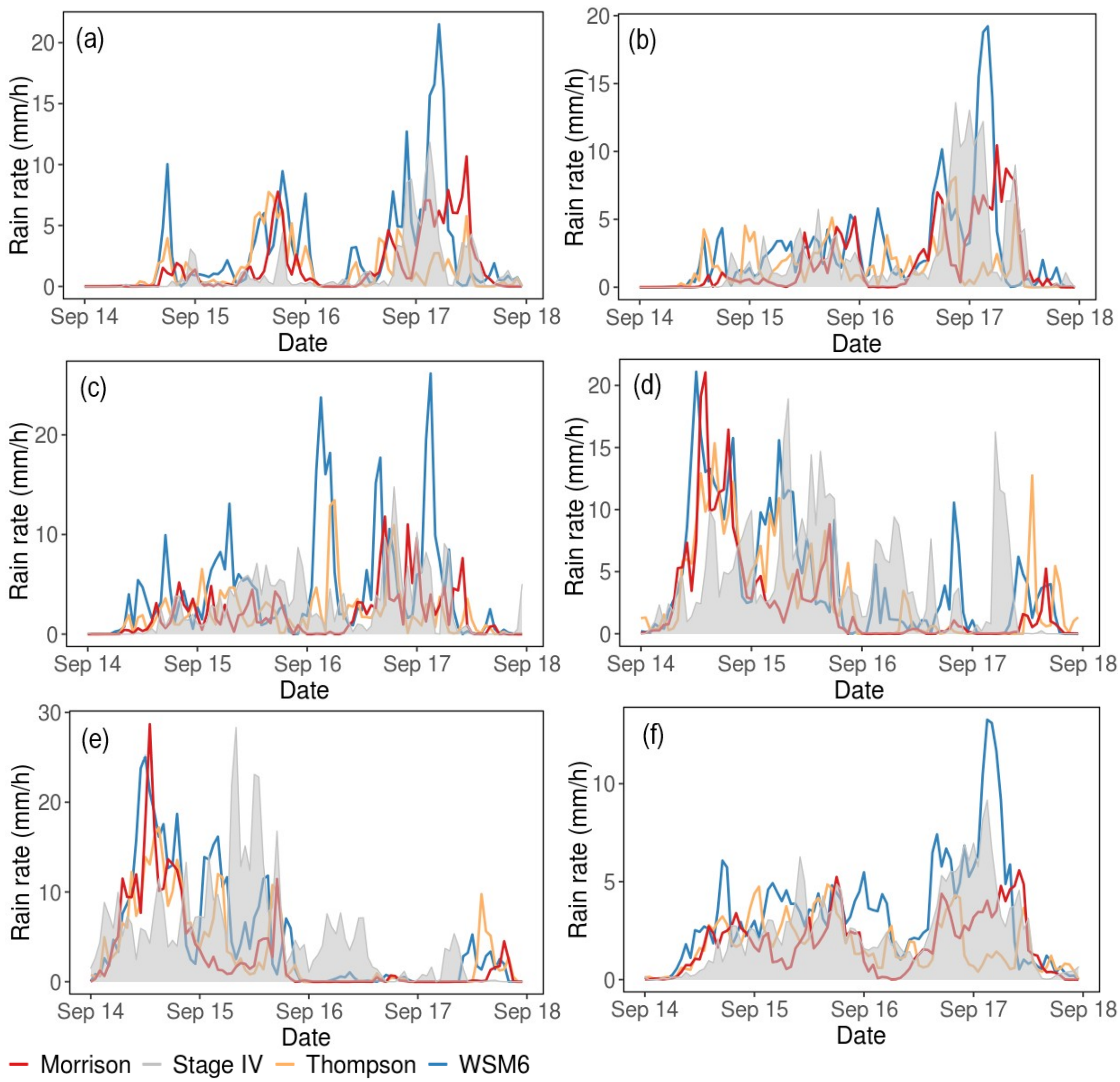

Figure 13. Time series of hourly areal rainfall rate during Florence (09/14 0000-09/18 0000 2018) over areas gaged by USGS Gage (a) 02096960 along the Haw River, (b) 02102000 along the Deep River, (c) 02103000 along the Little River, (d) 02106500 along the Black River, (e) 02108000 along the Northeast Cape Fear River, (f) 02105769 along the mainstem of the Cape Fear River from WRF simulation with WSM6 scheme (OFF1, solid blue line), Thompson scheme (OFF2, solid yellow line) and Morrison scheme (OFF3, solid red line) as well as Stage IV (grey shaded area). The locations of the gages are shown in Figure 1b.

731

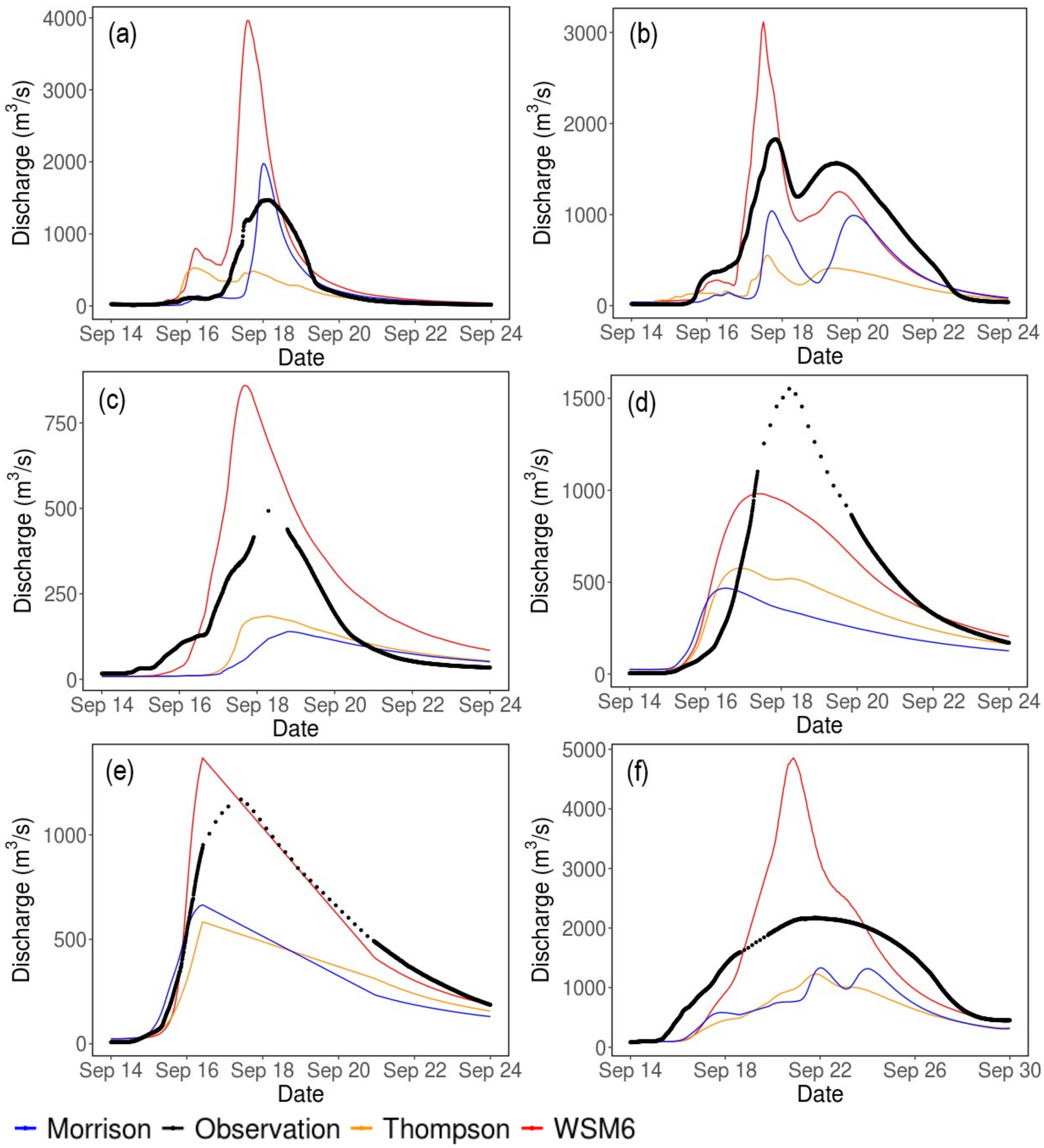

Figure 14. Simulated (WSM6: red, Thompson: orange, Morrison: blue) and observed (black dot) hydrographs for: (a) the Haw River basin at Bynum (USGS gage 02096960), (b) the Deep River basin Moncure (USGS gage 02102000), (c) the Little River basin Manchester (USGS gage 02103000), (d) the Black River basin Tomahawk (USGS gage 02106500), (e) the NE Cape Fear River Chinquapin (USGS gage 02108000) and (f) the mainstem of Cape Fear River at Kelly (USGS gage 02105769). The locations of the gages are shown in Figure 1b. Statistical performance are shown in Table 6.

732